Inner-shell excitation spectroscopy of aniline, nitrobenzene, and nitroanilines

Cássia C. Turci, Stephen G. Urquhart, and Adam P. Hitchcock

Abstract: Oscillator strengths for C 1s, N 1s, and O 1s excitation spectra of aniline, nitrobenzene, and the isomeric nitroanilines have been derived from inner-shell electron energy loss spectroscopy recorded under low momentum transfer conditions (>2.5 keV impact energy and small scattering angle, $\theta \leq 2°$). Extended Hückel Molecular Orbital (EHMO) calculations carried out within the equivalent core analogy are used to aid spectral interpretation. These spectra are used to investigate the sensitivity of core excitation spectroscopy to charge transfer interactions in aromatic molecules that have both electron-donating and electron-withdrawing substituents. Strong multielectron excitation features were not found, although these had been anticipated from photoemission studies. The C 1s $\rightarrow \pi^*$ and N 1s (NH_2) $\rightarrow \pi^*$ spectral features of the nitroanilines are found to be strongly dependent on the substitution pattern (*ortho*, *meta*, or *para*).

Key words: electronic structure, inner-shell excitation, nitroanilines, EHMO calculations.

Résumé : En se basant sur la spectroscopie de la perte d'énergie des électrons des couches internes dans des conditions de faible transfert du moment (énergie d'impact >2,5 keV et faible angle de diffusion, $\theta \leq 2°$), on a dérivé les forces d'oscillateur des C 1s, N 1s et O 1s pour les spectres d'excitation de l'aniline, du nitrobenzène et des nitroanilines isomères. Comme aide à l'interprétation spectrale, on a utilisé des calculs d'orbitales moléculaires de Hückel étendues (OMHE) effectués à des conditions correspondantes à celle de l'analogie équivalente à celles des couches internes. On a utilisé ces spectres pour étudier la sensibilité de la spectroscopie d'excitation des couches intérieures aux interactions de transfert de charge dans des molécules qui portent à la fois des substituants électrodonneurs et électroattracteurs. On n'a pas observé de caractéristiques de fortes excitations multiélectroniques, même si on les avait anticipées sur la base des études de photoémission. On a observé que les caractéristiques spectrales des transitions C 1s $\rightarrow \pi^*$ et N 1s (NH_2) $\rightarrow \pi^*$ des nitroanilines dépendent fortement des positions (*ortho*, *méta* ou *para*) des substituants.

Mots clés : structure électronique, excitation des couches intérieures, nitroanilines, calculs d'OMHE.

[Traduit par la rédaction]

I. Introduction

This study was motivated by observations in the early 1980s of intense satellite structures in the N 1s X-ray photoelectron spectra of gas phase and condensed *para*-nitroaniline and related compounds (1–11). The X-ray photoelectron spectrum (XPS) of solid *para*-nitroaniline exhibits a single sharp line attributed to N 1s(NH_2)[2] ionization and a 2 eV doublet with approximately equal intensity components initially attributed to N 1s(NO_2) ionization. Early interpretations (1) suggested that the lower binding energy component of the two peaks attributed to N 1s(NO_2) ionization was actually a multiconfigurational state in which N 1s(NO_2) ionization combined with a $\pi \rightarrow \pi^*$ excitation resulted in a state at *lower* energy than that of the one-electron N 1s(NO_2) ionization i.e., a *shake-down* satellite. This unusual situation was ascribed to a facile intramolecular charge transfer in this classic push–pull, donor–acceptor species. However, the N 1s XPS spectrum of gas phase *para*-nitroaniline was found to have a single broad N 1s(NO_2) peak (2) that, upon better resolution, was shown to consist of an asymmetric peak structure (6). Further work involving comparisons of vapour and solid state XPS spectra of *para*-nitroaniline (2, 6, 9, 11), and quantum calculations (4–6, 12) led to alternate spectral interpretations, including a more conventional *shake-up* picture in which the main line, one-electron N 1s(NO_2) ionization was attributed to the lower energy component of the doublet and the intense satellite at 2 eV higher energy was attributed to a (NH_2) $\rightarrow$ (NO_2) charge-transfer satellite of the N 1s(NH_2) line. Differences between the gas and solid state N 1s XPS were attributed to intermolecular charge transfer (9, 10, 12, 13) or hydrogen bonding effects in the solid (6).

The presence of the intense shake (charge transfer) satellites in the N 1s (and to a lesser extent, the O 1s) XPS led us to wonder whether the donor–acceptor character of disubstituted benzenes such as nitroaniline might give rise to analogous intense multielectron satellite structures in the core excitation spectra. Core excitation spectra might be expected to show satellite features closely related to those in core ionization

Received September 20, 1995.

This paper is dedicated to Professor Richard F.W. Bader on the occasion of his 65th birthday.

C.C. Turci. Instituto de Química, Universidade Federal do Rio de Janeiro, Rio de Janeiro, RJ, Brazil, 21910-900 and Department of Chemistry, McMaster University, Hamilton, ON L8S 4M1, Canada.

S.G. Urquhart and A.P. Hitchcock.[1] Department of Chemistry, McMaster University, Hamilton, ON L8S 4M1, Canada.

[1] Author to whom correspondence may be addressed. Telephone: (905) 525-9140, ext. 24749. Fax: (905) 521-2773. E-mail: aph@mcmaster.ca

[2] The core level involved is indicated by this notation. The character of the upper level of a given transition is indicated by a subscript, e.g., π^*_{NO}.

when the same core hole is involved. However, the discrete core excited states are neutral and the excited electron can have strong shielding effects such that the electron reorganization (charge transfer) that leads to XPS satellite lines may be strongly suppressed. Thus, rather than dramatic shake-up features analogous to those seen in XPS, there might be threshold onsets at the energy of the XPS shake-up signal superimposed on other spectral features in the continuum region of the core excitation spectrum (similar to those identified in the core spectra of some simple molecules such as CO and N_2 (14)), but there may not be any strong, sharp-line, multi-electron excitations built upon the main 1s $\rightarrow \pi^*$ discrete transitions. The initial motivation of our study was then to determine which of these two scenarios the experimental spectrum most resembled.

Another interesting theme of the core excitation spectroscopy of these molecules is the dependence of the C 1s $\rightarrow \pi^*$ structure on the nature of the disubstitution pattern (*ortho* versus *meta* versus *para*). While the core excitation spectra of several homo disubstituted benzenes have been studied previously (15, 16), to our knowledge this is the first study of the core spectra of a hetero disubstituted benzene. The pattern of unoccupied π^* orbitals will be affected by π^* electronic interaction between the NH_2 and NO_2 substituents through the ring-π^* system which, in turn, will depend on the substitution pattern. This, along with changes in the C 1s chemical shifts, should be reflected in the C 1s $\rightarrow \pi^*$ signals. If a characteristic signature for *ortho*, *meta*, and *para* substitution patterns can be identified, this could be useful with regard to analytical applications of NEXAFS spectroscopy, such as polymer microanalysis (16, 17).

In this work, inner-shell electron energy loss spectroscopy (ISEELS) has been used to record the C 1s, N 1s, and O 1s spectra of the three isomeric nitroanilines. In addition, the core spectra of nitrobenzene and aniline have been measured, in order to use spectral comparisons to aid assignment. The experimental conditions (high impact energy and small scattering angle) are such that the ISEELS spectra are expected to exhibit the same spectral features with similar relative intensities as those of the corresponding photoabsorption spectra. To our knowledge, aniline is the only one of these species for which core excitation spectra have been reported earlier (18–20), namely, X-ray absorption (NEXAFS) studies of the condensed multilayer solid.

The experimental spectra are reported on absolute oscillator strength scales using a previously developed conversion scheme (21). Extended Hückel (EHMO) calculations and a simple semiempirical molecular orbital method (22–24), carried out within the equivalent ionic core virtual orbital model (EICVOM) (25, 26), have been used to assist spectral assignments and to explore aspects of the virtual molecular orbital electronic structure of these species.

II. Experiment

The gas phase ISEELS spectrometer employed in these experiments has been described in detail previously (27). Basically, it is a high-vacuum apparatus consisting of an electron gun, sets of electrostatic deflector plates for beam steering, beam current monitors, a gas cell, a post collision deceleration lens, a hemispherical electrostatic energy analyzer, and a single electron counting detection system. The detector pulses are processed by standard electronics (preamplifier, amplifier, discriminator) and are counted by a microcomputer that also scans the analyzer voltages and stores the acquired data. The spectrometer is operated under conditions of small momentum transfer where the electronic excitations are dominated by electric-dipole-allowed transitions. The impact energy is 2.5 keV plus the energy loss and the scattering angle is ~2°C. The overall spectral resolution was typically in the range of 0.6–0.8 eV full width at half maximum (fwhm), although the C 1s spectrum of aniline was recorded with a resolution of 0.45 eV.

All samples were obtained commercially; aniline from BDH, nitrobenzene from Baker, and nitroanilines (*ortho*, *meta*, *para*), from Eastern. All samples had a stated purity better than 98%. They were run without further purification, except aniline and nitrobenzene, which were submitted to multiple freeze–pump–thaw cycles to remove any dissolved impurity gases or highly volatile components prior to their use. The least volatile samples, *para*-nitroaniline (mp 149°C), *meta*-nitroaniline (mp 114°C), and *ortho*-nitroaniline (mp 75°C) were placed inside a small glass tube attached directly to the collision cell of the spectrometer. For the *para* and *meta* compounds, the tube was gently heated with an internally mounted quartz–halogen bulb, while the end plates of the gas cell were water cooled to trap the vaporized sample and avoid insulating deposits on sensitive parts of the spectrometer. The aniline and nitrobenzene samples were sufficiently volatile to be introduced into the gas cell through a leak valve from a flask at low vacuum. Multiple spectra were obtained to confirm reproducibility.

The energy-loss scale was calibrated by recording the spectrum of a mixture of the unknown and a suitable reference molecule. The C 1s and O 1s spectra were calibrated using the C 1s $\rightarrow \pi^*$ (290.74(4) eV) (28, 29) and the O 1s $\rightarrow \pi^*$ (535.4(2) eV) (30) transitions of CO_2. The N 1s spectra were calibrated using the N 1s $\rightarrow \pi^*$ (401.10(2) eV) transition of N_2 (28, 29). The signal associated with a particular core edge was isolated from the underlying valence-shell ionization continuum by subtracting a smooth curve determined from a curve fit of the function $a(E - b)^c$ to the pre-edge experimental signal. These background subtracted spectra were then converted to absolute oscillator strength scales using a method described and tested previously (21).

III. EHMO calculations

Extended Hückel molecular orbital (EHMO) calculations were used to predict the core excitation spectra using the equivalent ion core virtual orbital model (EICVOM) (25, 26), as described previously (31–33). In the EICVOM method the localization and reorganization effects associated with core excitation are simulated by replacing the core excited atom with the element of one larger nuclear charge (the equivalent core approximation) and the valence electron count is corrected by adding a positive charge. The virtual orbital energies of the ground state of the cation are interpreted as the relative energies (approximate term values) of core $\rightarrow$ valence excited states while the intensities of each transition are assumed to be proportional to the sum of the square of the coefficients of the electric dipole coupled (2p) atomic orbitals on the 1s excited atom for each virtual MO (Σc^2_{N2p} for C 1s excitation, Σc^2_{O2p}

for N 1s excitation, and Σc^2_{F2p} for O 1s excitation). Extended Hückel calculations were performed with the CACAO molecular program (34) using the default EHMO parameters. The CACAO program provides pictures of the orbitals involved in the transitions that help to identify the spatial characteristics of the core excited electron density. The molecular geometries used in the calculation were ground-state experimental geometries taken from the literature (35).

To account for site-dependent core-hole localization effects on the virtual MOs (15) and the different chemical shifts in the 1s energies, the EHMO calculation of each spectrum is constructed from the results of calculations of the equivalent core analogy species with the core hole at all possible distinguishable sites (e.g., for *para*-nitroaniline, four distinct C 1s sites and two distinct N 1s sites). The core excitation spectrum for each site is constructed from the MO coefficients of all of the unoccupied MOs, with a peak at each eigenvalue assigned an area equal to the 2p density at the core excited atom (as given by twice the reduced charge matrix element (33)) and a width related to the eigenvalue. The experimentally observed line widths have been used as a guide to selecting fixed line widths in four ranges of eigenvalues, with gradually increasing line widths to account for the decreasing lifetime of higher energy continuum states.

Two procedures were explored for matching the EHMO to the absolute experimental energy scale. In the first one the zero of the eigenvalue scale for each component was set to the measured or estimated ionization potential (IP) (2, 36). The components were then added and the sum was shifted to match experiment at the prominent lowest energy π^* resonance. In the second procedure each site spectrum was placed on an absolute excitation energy scale by setting the strongest 1s $\rightarrow$ π^* feature in each site spectrum to the energy of the assigned experimental feature (table 8 provides details). The weighted sum of the individual site spectra (e.g., for C 1s in nitrobenzene, a 2:2:1:1 sum of C 1s(2,6), C 1s(3,5), C 1s(4), and C 1s(C-NO_2); see Fig. 2) was then the EHMO 1s spectrum for that species. The intensity of the EHMO spectrum was then scaled so that the integrated 1s $\rightarrow$ π^* intensity for experiment and EHMO was the same. To simulate the nonresonant part of the spectrum, an oscillator strength continuum component, generated from the tabulated values for the atom (37), was added. The second procedure, that in which the components are matched individually to experiment, gave more satisfactory agreement with experiment. This approach was used to calculate the spectra of each core level of all five molecules (a total of 14 predicted spectra).

IV. Results

A. C 1*s* spectra

A.1 Aniline and nitrobenzene: monosubstituted models

The main features of the C 1s spectra of all five molecules of this study can be readily related to those of benzene (38). First we discuss the spectra of the two singly substituted benzenes, which act as models for the nitroanilines. Figure 1 compares the C 1s spectra of aniline and nitrobenzene with that of benzene. The energies, term values, and proposed assignments of the spectral features of aniline are presented in Table 1 along with results from the literature (19, 20), while the values for

Fig. 1. C 1s oscillator strength spectra of aniline and nitrobenzene, compared to that of benzene (38). All of the spectra were derived from energy loss spectra recorded under near-dipole scattering conditions (2800 eV impact energy, 2° scattering angle) with 0.7 eV fwhm resolution. The hatched lines indicate the measured IPs (36). The insert is an expansion and curve fitting of the first π^* peak in nitrobenzene.

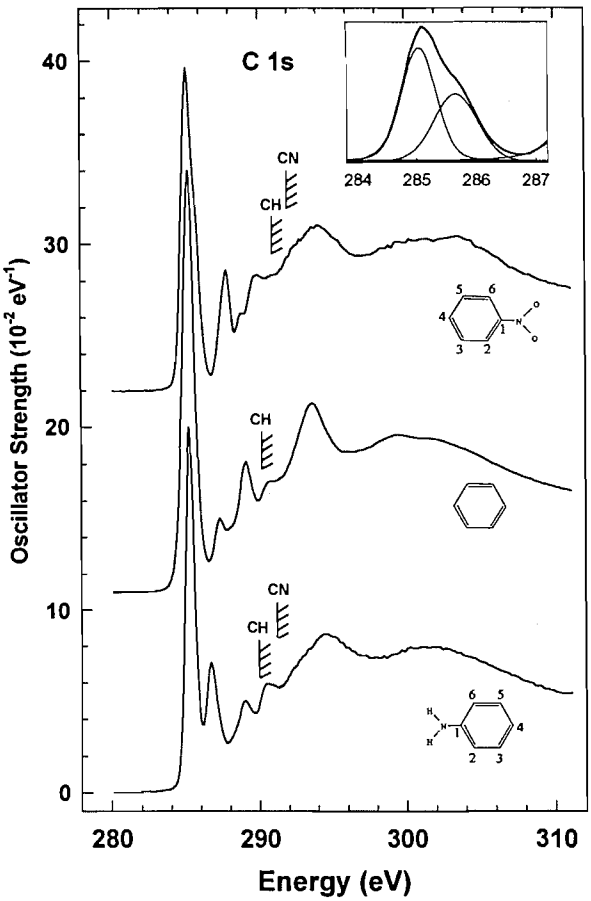

nitrobenzene are presented in Table 2. (Note that the tables only list the spectral features that can be readily observed in the accompanying figures. A number of weaker shoulders, which can be detected on closer examination, have not been tabulated. Our orientation in this study is to explain the main features and their chemical trends. We believe an exhaustive interpretation of all core excitation features is best delayed until higher resolution data are acquired).

Since the orbitals of the amine group interact very little with those of the π manifold, the C 1s $\rightarrow$ π^* region of aniline should be relatively similar to that of benzene, modified mainly by the chemical shift of the C 1s(C-N) site and possibly by a splitting of the e_{2u} ($\equiv 1\pi^*$) orbital of benzene. The lowest energy peak in the C 1s spectrum of aniline is a relatively narrow symmetric line (0.8 eV fwhm) while there is a second band at 1.5 eV higher energy. Based on the similarity of the separation of these first two bands to the separation of the C 1s(C-H) and C 1s(C-N) IPs (1.0 eV (36)), we attribute the second component to the C 1s(C-N) $\rightarrow$ $1\pi^*$ transition. The third resolved peak, that at 289.0 eV, is attributed to the C 1s(C-H) $\rightarrow$ $2\pi^*$ transition (correlating with the b_{2g} ($\equiv 2\pi^*$)

Table 1. Energies (eV), term values (eV), and proposed assignments for features in the 1s spectra of aniline.

(*a*) C 1s.

Gas (this work)		Solid (NEXAFS)		Term value[a]		Assignment	
No.	E (±0.1 eV)	E^b(eV)	E^c(eV)	T_{CH}	T_{CN}	C-H	C-N
1	285.2[d]	285.4	285.4	5.0		$1\pi^*(4b_1)$[e]	
2	286.7	286.9	286.8		4.6		$1\pi^*(4b_1)$
3	289.0	288.7		1.2		$2\pi^*(5b_1)$/3p	
4	290.5	290.6			0.8		$2\pi^*(5b_1)/\sigma^*_{CNH}$
IP	290.2[f]					IP	
IP	291.3[f]						IP
5	294.5	294.5		−3.7		$1\sigma^*$	
6	302(1)	303		−11		$2\sigma^*$	

(*b*) N 1*s*.

No.	*E* (±0.1 eV)	TV	Assignment
1 (sh)	400.7	4.6	3s
2	402.2[d]	3.1	$3p/\pi^*_{NH}(4b_1)$
3 (br)	404	1.3	σ^*_{NH}
IP	405.3[f]		IP
4	407.6	−2.3	σ^*_{CN}

[a]TV = E − IP (derived using values for gas phase excitation energies).
[b]From ref. 19, C 1s spectrum of solid aniline, a multilayer on Ag (110).
[c]From ref. 20.
[d]Calibration: C 1s −5.51(3) eV relative to CO_2 (π^*); N 1s +1.1(1) relative to N_2 (π^*).
[e]Solomon et al. (19) attribute the first feature to a combination of $\pi^*(2a_2)$ and $\pi^*(4b_1)$ excitations. Otherwise all other assignments are the same as given above.
[f]IPs from ref. 36.

orbital of benzene). There is debate concerning the assignment of the corresponding feature in benzene. Both experimental and theoretical studies provide evidence that the final state at 289 eV in benzene is one in which the one-electron (C $1s^{-1}$, $\pi^*(b_{2g})$) configuration is heavily mixed with the (C $1s^{-1}$, π^{-1}, π^{*2}) multi-electron excited configuration (39–41). By analogy to benzene, it is likely that the 289 eV feature in aniline may also contain contributions from multi-electron (C $1s^{-1}$, π^{-1}, π^{*2}) excitations. We do not see any evidence in the aniline C 1s spectrum for the splitting of the $1\pi^*(e_{2u})$ into $2a_2$ and $4b_1$ levels, expected from the reduction of symmetry from that of benzene. According to the electron transmission spectrum of aniline (42) this splitting is of the order of 0.5 eV, which should be detectible. However, transitions to the $2a_2$ orbital are found from quantum calculations to have negligible intensity (see Sect. A.2).

The situation is rather different in nitrobenzene since the π and π^* orbitals of the nitro group interact with those of the ring. Essentially, four π^* orbitals must be considered in the spectral assignments of the C 1s spectrum of nitrobenzene (and also in the nitroanilines) — the three intrinsic π^* orbitals of the ring plus the π^*_{NO} — whereas only the three π^* orbitals of the ring are involved in aniline. While the nitrobenzene spectrum superficially resembles that of benzene, in fact there are marked differences. In particular, if the C 1s spectrum was analogous to that of aniline there should be a C 1s(C-N) → $1\pi^*$ peak around 286.1 eV, about 1 eV above the main C 1s(C-H) → π^* line at 285.1 eV since the C 1s(C-H)/C 1s(C-N) chemical shift is 1.0 eV (36). No such peak exists. However, there is a high-energy shoulder on the first peak, with a separation of 0.64 eV (see the insert to Fig. 1), which is effectively the C 1s(C-N) → $1\pi^*$ transition, but with a significant shift to lower energy because of mixing of the $1\pi^*_{C=C}$ and π^*_{NO} orbitals. In fact, the EHMO calculations (see next section) indicate that interaction of the $1\pi^*_{C=C}$ and π^*_{NO} orbitals has a major effect on all of the C 1s → π^* transitions, such that the second, fully resolved peak in the C 1s spectrum of nitrobenzene (287.8 eV) also arises from C 1s(C-H) → $1\pi^*/\pi^*_{NO}$ transitions. The C 1s → $2\pi^*$ transitions are relatively unchanged from those in benzene and aniline and are attributed to the peak at 288.8 eV and part of the broader signal at 289.7 eV.

At higher energy, the C 1s continua of aniline and nitrobenzene are relatively similar, each exhibiting a two-peaked pattern very similar to that of benzene (38). These features are attributed to C 1s → σ^*_{C-C} transitions. According to the bond length correlation (43), which relates the position of 1s → σ^*_{XY} transitions referenced to the ionization threshold to the X—Y bond length, there should also be C 1s → σ^*_{CNH} (aniline) and C 1s → σ^*_{CNO} (nitrobenzene) features appearing around 291 eV. Broader structures in this region are so assigned in each species. The term value of the σ^*_{CN} feature in aniline is 1.6 eV smaller than that in nitrobenzene, consistent with the shorter C—N bond length in aniline (1.431 Å) than that in nitrobenzene (1.478 Å) (43).

A.2 EHMO results for aniline and nitrobenzene

Table 3 summarizes a selection of the EHMO results for the π^* resonances for aniline and nitrobenzene. Figure 2 com-

Table 2. Energies (eV), term values (eV), and proposed assignments for features in the 1s spectra of nitrobenzene.

(*a*) C 1s.

No.	Energy (±0.1 eV)	Term value T_{CH}	Term value T_{CN}	Assignment $C_{2,6}$-H	Assignment $C_{3,5}$-H	Assignment C_4-H	Assignment C_1-N
1	285.1[a]	6.0		$1\pi^*(4b_1)$	$1\pi^*(5b_1)$	$1\pi^*(4b_1)$	
2 (sh)	285.7		6.4				$1\pi^*(5b_1)$
3	287.8	3.3		$1\pi^*(5b_1)$		$1\pi^*(5b_1)$	
4	288.8		3.3		$2\pi^*(6b_1)$		
5	289.7		2.4	$2\pi^*(6b_1)$		$2\pi^*(6b_1)$	$2\pi^*(6b_1)$, σ^*_{CNO}
IP	291.1[b]			IP	IP	IP	
IP	292.1[b]						IP
6	294.0	−2.4		←	$1\sigma^*$	→	
7	302(1)	−10		←	$2\sigma^*$	→	
8	328(2)	−36			EXAFS		

(*b*) N 1s.

No.	Energy	TV	Assignment
1	403.8[a]	7.7	π^*_{NO}
2	408.3	3.2	$3p/\pi^*_{mix}$[c]
3	409.5	2.0	4p
IP	411.5[b]		IP
4	413.2	−1.7	σ^*_{CN}, $\sigma^*_{NO}(+)$
5	418.5(3)	−7	$\sigma^*_{NO}(-)$

(*c*) O 1s.

No.	Energy	TV	Assignment
1	530.9[a]	7.6	π^*_{NO}
2	534.0	4.5	π^*_{mix}[c]
3	538.0	0.5	$\sigma^*_{NO}(-)$
IP	538.5[b]		IP
4	541.3	−2.8	$\sigma^*_{NO}(+)$

[a]Calibration: C 1s −5.65(3) eV; N 1s +2.67(2) relative to N_2 π^*; O 1s −4.46(6) eV relative to CO_2 π^*.

[b]IPs from ref. 36.

[c]π^*_{mix} refers to a higher energy MO of π^* symmetry with both π^*_{NO} and $\pi^*_{C=C}$ character.

pares the experimental C 1s spectrum of nitrobenzene with that predicted from the EHMO-EICVOM calculations. In addition to illustrating the methodology used to align the individual site components with experimental data, this figure nicely reveals the important role of $\pi^*_{C=C}$ and π^*_{NO} orbital mixing in the C 1s spectrum. According to EHMO, the main π^* contribution for C_1 and $C_{3,5}$ excitations is from the $\pi^*(5b_1)$ orbital, which is an admixture of the π^*_{NO} and $\pi^*_{C=C}$ orbitals. However, at both the C_4 and $C_{2,6}$ sites, there is significant contribution from both the $4b_1$ and $5b_1$ orbitals, with each of these MOs having a combined $\pi^*_{C=C}$ and π^*_{NO} character. There is no significant contribution from the $3a_2$ component (derived from splitting of the e_{2u} orbital of benzene) at any C 1s site. At higher energy there is a small contribution from C 1s $\pi^*(6b_1)$ transitions at each site. Thus, EHMO suggests that the relatively simple experimental spectrum arises from the C 1s(C-H)/C 1s(C-N) chemical shift and a complex overlap of transitions to the $4b_1$ and $5b_1$ orbitals, which have a site-dependent mix of $\pi^*_{C=C}$ and π^*_{NO} character.

As illustrated in Fig. 2, the EHMO predictions for nitrobenzene are in reasonable agreement with experiment in the π^* region (284–288 eV). There is less satisfactory agreement in the region of the continuum onset (288–291 eV), in part because EHMO cannot reproduce spatially extended Rydberg states. There is also disagreement between calculation and experiment in the region of the continuum resonances (and this is true for all species of this study). These resonances are related to 1s excitations to high-lying σ^* MOs, which in some cases have a relatively localized character associated with specific structural aspects of the molecule (43). EHMO often predicts the correct pattern of high-energy σ^* features, but typically places the σ^* resonances at higher energies and with significantly distorted intensities. This could be related to inadequacies of EHMO and other semi-empirical quantum

Table 3. Energies and LCAO-MO coefficients at the core excited atom in π* orbitals of aniline and nitrobenzene from EHMO-EICVOM calculations.

Aniline

MO sym	*E*(eV) ground state	N 1s		MO sym[a]	C 1s(2, 6)		C 1s(3, 5)		C 1s(4)		C 1s(C-N)	
		E	c^2(O2p)		*E*	c^2(N2p)	*E*	c^2(N2p)	*E*	c^2(N2p)	*E*	c^2(N2p)
$5b_1$	4.42	4.51	0.004	$5b_1(2\pi^*)$	5.10	0.029	4.97	0.023	4.94	0.021	5.25	0.031
$4b_1$	7.86	8.04	0.011	$2a_2(1\pi^*)$	7.91	0.002	7.97	0.002	8.29	0.000	8.29	0.000
$2a_2$	8.29	8.29	0.000	$4b_1(1\pi^*)$	9.20	0.095	9.38	0.121	9.00	0.109	9.17	0.137

Nitrobenzene

MO sym	*E*(eV) ground state	O 1s		N 1s		MO sym	C 1s(2, 6)		C 1s(3, 5)		C 1s(4)		C 1s(C-N)	
		E	c^2(F2p)	*E*	c^2(O2p)		*E*	c^2(N2p)	*E*	c^2(N2p)	*E*	c^2(N2p)	*E*	c^2(N2p)
$6b_1$	4.55	4.55	0.001	4.67	0.004	$6b_1(2\pi^*)$	5.21	0.029	5.09	0.022	5.05	0.020	5.37	0.031
$5b_1$	7.81	7.84	0.003	8.11	0.014	$3a_2(1\pi^*)$	7.85	0.002	7.94	0.004	8.35	0.000	8.35	0.000
$3a_2$	8.35	8.35	0.000	8.35	0.000	$5b_1(1\pi^*, \pi^*_{NO})^b$	9.17	0.076	9.41	0.119	8.84	0.089	9.01	0.124
$4b_1$	10.56	10.83	0.024	11.86	0.201	$4b_1(\pi^*_{NO}, 1\pi^*)^b$	10.80	0.040	10.56	0.000	10.82	0.043	10.57	0.003

[a] $\{\pi^*(2a_2), \pi^*(4b_1)\}$ correlates with the e_{2u} orbital while $2\pi^*(5b_1)$ correlates with the b_{2g} orbital in benzene.
[b] The $4b_1$ and $5b_1$ orbitals are a site-dependent mix of the b_1 component derived from the $1\pi^*$ (e_{2u}) and the $1\pi^*_{NO}$ (b_1) orbital of the NO_2 group.

Fig. 2. EHMO predicted C 1s spectrum of nitrobenzene compared to experiment. The full C 1s EHMO spectrum is the sum of the indicated constituent components and a nonresonant ionization signal estimated from that tabulated for atomic carbon (37), aligned at the C 1s IPs. The EHMO component spectra were aligned with experiment at the approximate position of the main π^* resonance, with exact values chosen to obtain the best visual agreement with experiment (see Table 8).

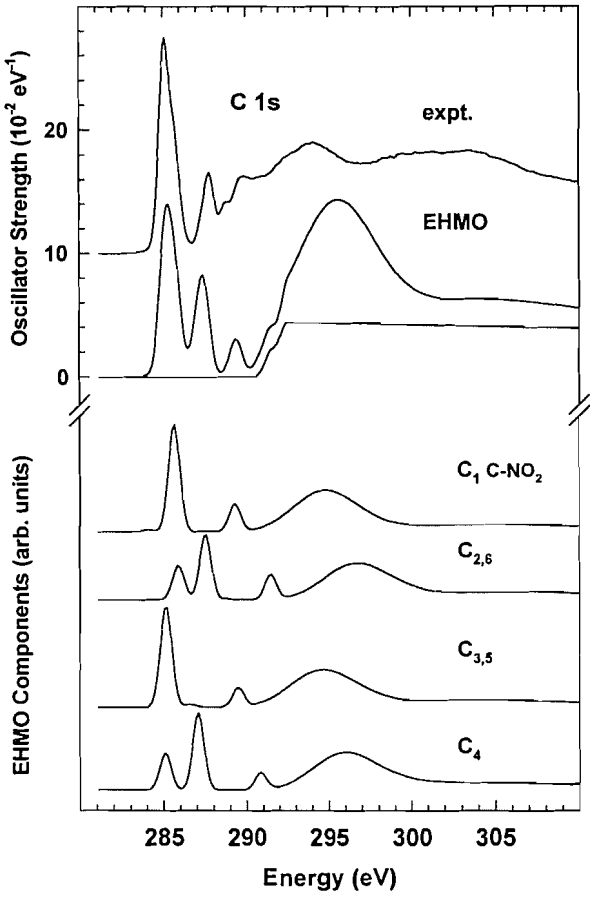

calculations (44) at treating high-energy molecular orbitals. Interestingly, while EHMO overestimates the energy of high-lying σ^* levels, CNDO (44) appears to predict the corresponding levels at energies below those observed experimentally.

The EHMO results for aniline (Table 3, Fig. 3) are a close match to the qualitative spectral description given in the preceding section. The C 1s spectrum of gaseous aniline presented in this work is very similar to the C 1s NEXAFS spectrum of a multilayer of solid aniline on Ag(110) (19). The energies and assignments of the spectral features are generally in agreement with the present work. Solomon et al. (19) and Luo et al. (20) attributed the peaks at 286.9 and 288.7 eV in the NEXAFS spectrum of solid aniline to the presence of the NH_2 group, which, leads to chemical shifts in the C 1s levels and lifts the degeneracy of the $1\pi^*(e_{2u})$ molecular orbitals of benzene. The NEXAFS spectrum of solid aniline has been interpreted by Luo et al. (20) on the basis of high-level multiconfigurational self-consistent field (MCSCF) calculations, in which both relaxation and correlation effects are taken into account. One notable difference among these three studies of C 1s excited aniline is that we and Luo et al. (20) attribute the

Fig. 3. (*a*) C 1s spectra of aniline, the isomeric nitroanilines, and nitrobenzene in the region of the C 1s $\rightarrow \pi^*$ excitation, predicted from EHMO calculations. See the text and Table 8 for details of the line widths and shifts used to construct the predicted spectra. (*b*) Corresponding region of the experimental C 1s oscillator strength spectra.

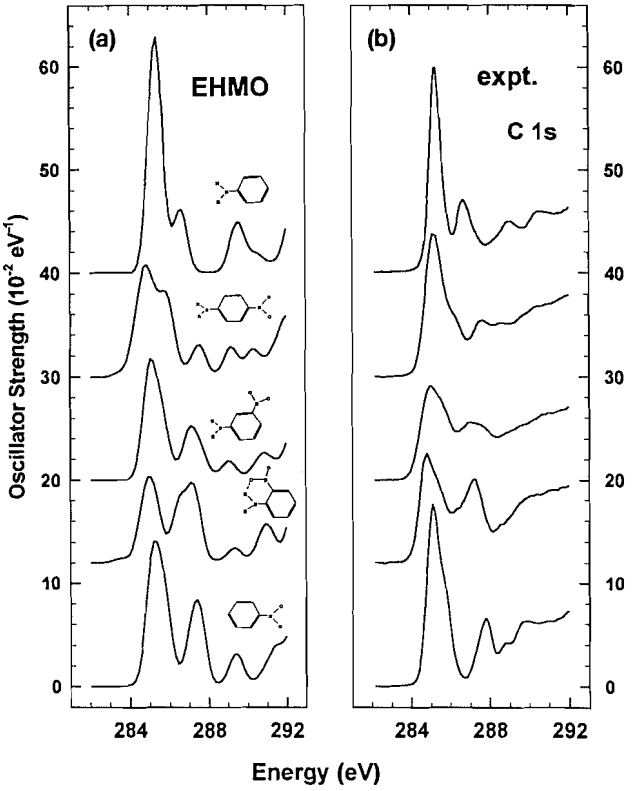

lowest energy peak to C 1s (C-H) $\rightarrow \pi^*$ $(4b_1)$ transitions whereas Solomon et al. (19) have attributed it to combined C 1s $\rightarrow \pi^*(2a_2)$ and C 1s $\rightarrow \pi^*(4b_1)$ transitions. Although C 1s $\rightarrow \pi^*(a_2)$ transitions are allowed at the $C_{2,6}$ and $C_{3,5}$ sites in C_{2v} symmetry, both the EHMO and MCSCF calculations indicate that these have negligible intensity (see Table 3). Another interesting aspect of the EHMO results for aniline (and nitrobenzene) is that there is a reversal in ordering of the a_2/b_1 components associated with the $1\pi^*_{C=C}$ orbital between the ground and N 1s/ O1s states (where $a_2 < b_1$), and all of the C 1s excited states (where $b_1 < a_2$) . The reversal occurs because the C 1s core hole stabilizes the $\pi^*_{C=C}(b_1)$ orbital by 1.1–1.4 eV (see Table 3), but not the a_2 orbital. The "avoidance" of the core hole by the a_2 orbital is the reason there is no contribution from C 1s $\rightarrow \pi^*(a_2)$ transitions. Thus, on the basis of both energetics and intensities, EHMO indicates the main C 1s $\rightarrow \pi^*$ intensity is associated with the b_1 orbitals and not the a_2 orbital.

Table 4 compares our C 1s EHMO predictions of the lower energy π^* features of aniline with those from the MCSCF calculations reported by Luo et al. (20). The MCSCF calculations also indicate that transitions to the $\pi^*(a_2)$ orbital have negligible intensities. They show that the lowest core excited state is the $\{C\ 1s(3, 5)^{-1}, \pi^*(4b_1)\}$ state, which is almost degenerate (ΔE = 0.03 eV) with the $\{C\ 1s(2, 6)^{-1}, \pi^*(4b_1)\}$ state. The energy shift of the $\{C\ 1s(3, 5)^{-1}, \pi^*(4b_1)\}$, $\{C\ 1s(4)^{-1}, \pi^*(4b_1)\}$, and $\{C\ 1s(C\text{-}N)^{-1}, \pi^*(4b_1)\}$ states relative to the

Table 4. Relative spacings of C 1s → π* transitions for aniline from experiment and calculation.

C 1s.

		EHMO calculation		Relative E		
C no.	IP(eV)[a]	−ε(eV)	E(eV)[b]	EHMO[c]	MCSCF (20)	Expt. (this work)
1(C-NH_2)	291.3	9.17	282.1	1.3	1.15	1.5
2,6	290.2	9.20	281.0	0.2	0.03	(<0.2)[d]
3,5	290.2	9.38	280.8	0	0	0
4	290.2	9.00	281.2	0.4	0.29	(<0.2)[d]

[a]From XPS (36).
[b]Assumes −ε from EHMO is equal to the term value. Typically this overestimates the transition energy by about 4 eV (see Table 8).
[c]E_{rel} is the energy relative to the C 1s(3, 5) → 1π*($4b_1$) transition.
[d]The splitting attributable to this separation is not detected. This value is an upper bound based on the 0.45 eV resolution of our ISEELS system and that of <0.2 eV in the NEXAFS study (20).

Fig. 4. C 1s oscillator strength spectra of the *ortho*-, *meta*-, and *para*-nitroaniline, compared to a simulation that is the sum of the C 1s spectra of nitrobenzene (shifted by −0.1 eV) and aniline (shifted +0.8 eV) minus that of benzene (shifted by +0.5 eV) (the shifts are the IP shifts). See Fig. 1 for experimental details.

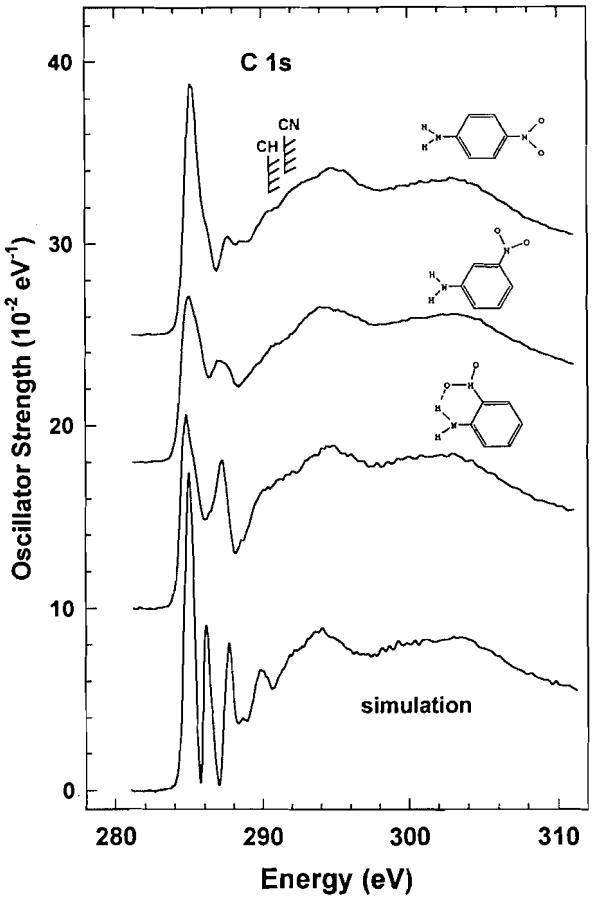

lowest core excited state are also presented in Table 4. Overall the EHMO results agree very well with those from MCSCF calculations. Based on the energy differences between different core-excited states, Luo et al. (20) assigned the first resonance (285.4 eV) to $C_{2,3,4}$ → π*($4b_1$) transitions and the second resonance (286.8 eV) to C 1s(C-N) → π*($4b_1$) transitions, as in the present work. Our calculations indicate that the 290.5 eV feature, which lies above the C 1s(C-N) IP, is the C 1s(C-N) → π*($5b_1$) transition, as first proposed by Solomon et al. (19).

A.3 C 1s spectra of nitroanilines

The C 1s spectra of the isomeric nitroanilines are presented in Fig. 4, while the energies, term values, and proposed assignments are given in Tables 5, 6, and 7. The C 1s chemical shifts of nitroanilines have not been measured although an average C 1s IP of 291.1 eV for *para*-nitroaniline has been reported (2). Based on this value and the shifts between the C 1s(C-H) and the C 1s(C-N) IPs of 1.1 eV for aniline and 1.0 eV for nitrobenzene, we estimate the C 1s IPs of all three nitroanilines as 290.8 eV (C 1s(C-H)) and 291.8 eV (C 1s(C-N)).

If there was negligible interaction between the nitro and amine groups, one might expect the C 1s spectra of the nitroanilines to be similar to a weighted sum of the C 1s spectra of aniline and nitrobenzene as proposed by the "building block" approach (18). Figure 4 includes a comparison to a simulation of the spectrum generated in this manner. The substantial difference between the simulation and any of the nitroaniline spectra in the region of the π* structure indicates that the two substituents interact electronically to affect the unoccupied π* structure. Thus the details of the C 1s spectra provide insight into the donor–acceptor (push–pull) interactions between the NH_2 and NO_2 groups, through their influence on the carbon 2p contributions to the π* orbitals. Because the π^*_{NO} and $\pi^*_{C=C}$ levels of the three nitroanilines will interact in a manner similar to that in nitrobenzene, the spectral features are best explained using the nitrobenzene assignments as a model.

We attribute the first band (285–286 eV) in each of the nitroanilines to C 1s(C-H) → 1π* transitions and the second band (286.5–288.5 eV) to the superposition of C 1s(C-N) → 1π* and C 1s(C-H) → 2π* transitions. Both bands are structured in all three molecules, which is likely the effect of chemical shifts in the C 1s IPs, as well as shifts in state energies associated with the influence of the core-hole location on the energy of the π* orbitals. The C 1s continuum shape in all three nitroanilines is rather similar and can be readily interpreted as the doubly peaked structure of benzene with additional contribution from C 1s → σ^*_{CNO}, σ^*_{CNH} transitions around 290–292 eV. Further details of the ($C\ 1s^{-1}$, π*) spec-

Table 5. Energies (eV), term values (eV), and proposed assignments for features in the 1s spectra of *ortho*-nitroaniline.

(*a*) C 1s.

No.	Energy (±0.1 eV)	Term value T_{CH}	Term value T_{CN}	Assignment[c] $C_{3,5}$-H	Assignment[c] $C_{4,6}$-H	Assignment[c] C_1-NO_2	Assignment[c] C_2-NH_2
1	284.9[a]	5.9		$1\pi^*(6b_1)$	$1\pi^*(5b_1)$		
2(sh)	285.3		6.5				$1\pi^*(5b_1)$
3(sh)	286.4	4.4			$1\pi^*(6b_1)$		
4	287.3		4.5			$1\pi^*(6b_1)$	$1\pi^*(6b_1)$
5(w)	288.6		3.2	$2\pi^*(7b_1)$, 3p			
6	290.5	0.3	1.3		$2\pi^*(7b_1)$	$2\pi^*(7b_1)$, σ^*_{CNO}	$2\pi^*(7b_1)$
IP	290.8[b]			IP	IP		
IP	291.8[b]					IP	IP
7	291.8(4)	0					σ^*_{CNH}
8	294.7		−3.4	←	$1\sigma^*$	→	
9	302(1)		−11	←	$2\sigma^*$	→	

(*b*) N 1s.

No.	Energy (±0.1 eV)	Term value T_{NH}	Term value T_{NO}	Assignment N-H	Assignment N-O
1	400.5	5.5		π^*_A[d]	
2	401.8	4.2		π^*_B[d]	
3 (sh)	403.0	3.0		3p	
4	403.8[a]		7.4		π^*_{NO}
IP	406.0[b]			IP	
5 (br)	406.5(9)	−0.5		σ^*_{CNH}	
6	409.2(5)		2		σ^*_{CNO}
IP	411.2[b]				IP
7	413.5		−2.3		$\sigma^*_{NO}(+)$
8	419		−8		$\sigma^*_{NO}(-)$

(*c*) O 1s.

No.	Energy	TV	Assignment
1	531.0[a]	6.9	π^*_{NO}
2(w)	534.0	3.9	π^*_{mix}[e]
IP	537.9[b]		IP
3	538.0	−0.1	$\sigma^*_{NO}(-)$
4	541.5	−3.6	$\sigma^*_{NO}(+)$

[a]Calibration: C 1s −5.83(3) eV; N 1s: +2.72(2) relative to N_2 π^*. O 1s −4.43(6) eV relative to CO_2 π^*.
[b]IPs estimated from those of *para*-nitroaniline (2).
[c]Symmetry labels from C_{2v} group.
[d]See Fig. 8 for sketches of these orbitals.
[e]π^*_{mix} refers to a higher energy MO of π^* symmetry with both π^*_{NO} and $\pi^*_{C=C}$ character.

tral assignments are provided by the EHMO results, which give insight into core-hole relaxation and delocalization effects.

Figure 3 plots an expansion of the experimental C 1s spectra for all five species in the π^* region between 284 and 290 eV, in comparison to the EHMO predictions. Table 8 lists the alignments that were used to generate each of the EHMO spectral predictions. If EHMO is a good tool for predicting core excitation on a relative energy scale, the "EHMO error" (SHIFT − IP) should be rather similar for all sites. Indeed the shifts are quite similar, with an average value of 4.1(1) eV, corresponding to a systematic overstabilization of the orbital energies, similar to that found for EHMO core excitation predictions in other systems (15, 32, 33). There are a few larger deviations, with the extrema of the EHMO errors being values of 2.2 and 5.5 eV for the C 1s(1) and C 1s(2) sites of *meta*-nitroaniline. It is possible these larger deviations are related to errors in the estimated IPs. Alternatively they may give insight into unusual, site-specific aspects of the electronic structure.

Figure 3 emphasizes that the C 1s → π^* signal varies con-

Table 6. Energies (eV), term values (eV), and proposed assignments for features in the 1s spectra of *meta*-nitroaniline.

(*a*) C 1s.

No.	Energy (±0.1 eV)	Term value T_{CH}	Term value T_{CN}	Assignment[c] $C_{2,4}$-H	C_5-H	C_6-H	C_1-NO_2, C_3-NH_2
1	285.1[a]	5.7		$1\pi^*(5b_1)$	$1\pi^*(6b_1)$	$1\pi^*(5b_1)$	
2(sh)	285.4		6.4				$1\pi^*(6b_1)$
3	286.8	4.0		$1\pi^*(6b_1)$		$1\pi^*(6b_1)$	
4	287.4		4.4				
5	289.6		2.2				$2\pi^*(7b_1)$
6	290.6	0.2	1.2	$2\pi^*(7b_1)$	$2\pi^*(7b_1)$		σ^*_{CNH},σ^*_{CNO}
IP	290.8[b]			IP	IP		
IP	291.8[b]					IP	IP
7	294.5		−3.3	←		$1\sigma^*$	→
8	304(1)		−13	←		$2\sigma^*$	→

(*b*) N 1s.

No.	Energy (±0.1 eV)	Term value T_{NH}	Term value T_{NO}	Assignment N-H	N-O
1	401.6	4.4		π^*_A[d]	
2 (sh)	402.5	3.5		π^*_B[d]	
3	403.6[a]		7.6		π^*_{NO}
IP	406.0[e]			IP	
4 (br)	406.2(9)	−0.2		σ^*_{CNH}	
5	408.5		2.7		σ^*_{CNO}
IP	411.2[e]				IP
6	412.8		−1.6		$\sigma^*_{NO}(+)$
7	418		−7		$\sigma^*_{NO}(-)$

(*c*) O 1s.

No.	Energy	TV	Assignment
1	530.9[a]	7.0	π^*_{NO}
2	534.0	3.9	π^*_{mix}
IP	537.9[b]		IP
3	538.0	−0.1	$\sigma^*_{NO}(-)$
4	541.2	−3.3	$\sigma^*_{NO}(+)$

[a]Calibration: C 1s −5.66(3) eV; N 1s: +2.52(2) relative to N_2 π^*; O 1s −4.52(6) eV relative to CO_2 π^*.

[b]C 1s and O 1s IPs estimated from those of *para*-nitroaniline.

[c]Symmetry labels from C_{2v} group.

[d]See Fig. 8 for sketches of these orbitals.

[e]N 1s IPs estimated from those of *p*-nitroaniline (2). The solid state XPS data (48) suggest the ΔIP N 1s (NO_2 – NH_2) of *meta* is 0.7 eV higher than that in *para*, with identical NH_2 IPs. However, this gives an unreasonably large term value for the π^*_{NO} state. Thus we believe the reported *meta–para* difference (48) is specific to the solid state, as suggested in comparisons of gas and solid paranitroaniline (11–13). We assume that the N 1s IPs of all three isomers are the same in the gas phase.

siderably with the substitution pattern. Some of these changes can be attributed to variations in the C 1s energies as the position of the two electronegative substituents changes. However, additional effects, in particular changes in the electronic communication between the two substituents, are clearly important factors. Overall EHMO gives good agreement with the experimental spectra, giving confidence that the relative orbital energies and LCAO compositions predicted by EHMO are reasonable. The orbital characters of the component lines give insight into spectral assignments, in particular addressing the roles of (*i*) the C 1s chemical shifts; (*ii*) the contributions of the "$1\pi^*$" and "$2\pi^*$"; (*iii*) the site-dependent mixing of the $\pi^*_{C=C}(b_1)$ and $\pi^*_{NO}(b_1)$ components, in setting the detailed spectral shape of the C 1s → π^* signals. It is important to observe that, although the symmetry of the ground state and excited state conformations of *ortho*- and *meta*-nitroaniline is

Table 7. Energies (eV), term values (eV), and proposed assignments for features in the 1s spectra of *para*-nitroaniline.

(*a*) C 1s.

No.	Energy (±0.1 eV)	Term value T_{CH}	Term value T_{CN}	Assignment[c] $C_{2,6}$-H	$C_{3,5}$-H	C_1-NO	C_4-NH_2
1	285.2[a]	5.6		$1\pi^*(5b_1)$	$1\pi^*(6b_1)$		
2	286.1		5.7			$1\pi^*(6b_1)$	$1\pi^*(5b_1)$
3	287.7	3.1		$1\pi^*(6b_1)$, 3p			
4	288.6	2.2	3.2		$1\pi^*(7b_1)$, 3p	$1\pi^*(7b_1)$, 3p	$1\pi^*(6b_1)$, 3p
5	290.2(4)	0.6	1.6	$2\pi^*(7b_1)$		σ^*_{CNO}	
IP	290.8[b]			IP	IP		
IP	291.8[b]					IP	IP
6	292.4	−0.6					$2\pi^*(7b_1)$, σ^*_{CNH}
7	294.5		−3.2	←	$1\sigma^*$	→	
8	303(1)		−12	←	$2\sigma^*$	→	

(*b*) N 1s.

No.	Energy (±0.1 eV)	Term value T_{NH}	Term value T_{NO}	Assignment N-H	Assignment N-O
1	401.6	4.4		π^*_A[c]	
2 (sh)	402.8	3.2		π^*_B[c]	
3	403.8[a]		7.4		π^*_{NO}
4 (sh)	405	1		4p	
IP	406.0[d]			IP	
5 (sh)	407.6(4)	−1.6		σ^*_{CNH}	
6 (br)	409.1		2.1		σ^*_{CNO}
IP	411.2[d]				IP
7	412.7		−1.5		$\sigma^*_{NO}(+)$
8	418		−7		$\sigma^*_{NO}(-)$

(*c*) O 1s.

No.	Energy	TV	Assignment
1	530.9[a]	7.0	π^*_{NO}
2	534.0	3.9	π^*_{mix}
IP	537.9[d]		IP
3	538	−0.1	$\sigma^*_{NO}(-)$
4	541.2	−3.3	$\sigma^*_{NO}(+)$

[a]Calibration: C 1s −5.55(3) eV; N 1s: +2.66(2) relative to N_2 π^*; O 1s −4.39(6) eV relative to CO_2 π^*.
[b]IPs derived from the average IP of 291.1 eV (2), the estimated C 1s(C-H)/C 1s(C-N) chemical shift, and the relative numbers of C-H and C-N ring carbons.
[c]See Fig. 8 for sketches of these orbitals.
[d]From XPS (2).

C_s, C_{2v}-based labels for the *para* isomer are used in the following discussion because of the similarity of the shapes of the C 1s MOs involved in the π^* transitions. As with nitrobenzene the EHMO component spectra indicate that the first four spectral features are a superposition of a number of 1s → $\pi^*(b_1)$ transitions at the distinct C 1s sites. In each case the $\pi^*(b_1)$ orbital has both $\pi^*_{C=C}$ and π^*_{NO} character. For C_1 (C-NO_2) and C_5 excitations in all three isomeric nitroanilines, C_3 excitation for *ortho*- and *para*-nitroaniline, and C-NH_2 excitation for the *meta* isomer, the C 1s → $\pi^*(6b_1)$ transition dominates. For the other sites (C_2 for *meta*- and *para*-nitroanilines, C_4 for *ortho*- and *meta*-nitroanilines, C-NH_2 for *ortho*- and *para*-nitroanilines, and the C_6 site for all nitroanilines) there is significant contribution from both the $6b_1$ and $5b_1$ orbitals. At higher energy there is a small contribution from C 1s → $7b_1$ ($2\pi^*$) transitions at all sites. In all three nitroanilines (as in nitrobenzene) the EHMO results suggest this $2\pi^*$ contribution comes about 0.5 eV higher in energy than in aniline or benzene. However these calculations do not take into account mixing with a doubly excited configuration ($C1s^{-1}$, π^{-1}, π^{*2}) that may shift the $2\pi^*$ transition to lower energy. The EHMO predicted spectra (Fig. 3) are consistent with our proposed

Table 8. Alignment of EHMO and experimental results.

(*a*) C 1s.

	Aniline			*para*-Nitroaniline			*meta*-Nitroaniline			*ortho*-Nitroaniline			Nitrobenzene		
C 1s	Shift[a]	IP[b]	Err[c]	Shift	IP	Err	Shift	IP	Err	Shift	IP	Err	Shift	IP	Err
1	295.7	291.3	4.4(NH_2)	294.7	291.8	2.9(NO_2)	294.0	291.8	2.2(NO_2)	296.2	291.8	4.4(NO_2)	294.4	292.1	2.3(NO_2)
2	294.6	290.2	4.4	295.2	290.8	4.4	296.3	290.8	5.5	296.2	291.8	4.4(NH_2)	296.7	291.3	5.4
3	294.6	290.2	4.4	294.3	290.8	3.5	295.0	291.8	3.2(NH_2)	293.9	290.8	3.1	294.5	291.0	3.5
4	294.6	290.2	4.4	296.1	291.8	4.3(NH_2)	295.8	290.8	5.0	295.3	290.8	4.5	295.9	291.2	4.8
5	294.6	290.2	4.4	294.3	290.8	3.5	294.0	290.8	3.2	293.9	290.8	3.1	294.5	291.0	3.5
6	294.6	290.2	4.4	295.2	290.8	4.4	295.9	290.8	5.1	295.4	290.8	4.6	296.7	291.3	5.4

(*b*) N1s and O 1s.

	Aniline			*para*-Nitroaniline			*meta*-Nitroaniline			*ortho*-Nitroaniline			Nitrobenzene		
Edge	Shift	IP	Err	Shift	IP	Err	Shift	IP	Err	Shift	IP	Err	Shift	IP	Err
N 1s(NO_2)	—	—	—	415.5	411.2	4.3	415.5	411.2	4.3	414	411.2	2.8	415.6	411.5	4.1
N 1s(NH_2)	410.0	405.3	4.7	410.0	406.0	4.0	409.4	406.0	3.4	409.8	406.0	3.8	—	—	—
O 1s	—	—	—	541.7	537.9	3.8	541.9	537.9	4.0	541.8	537.9	3.9	541.9	538.5	3.4

[a]The energy added to the EHMO eigenvalues to generate the absolute energy scale for this spectral component.

[b]From XPS or estimated. See Tables 1, 2, 5, 6, 7.

[c]Err = shift − IP. If EHMO eigenvalues were equal to negative term values this quantity would be 0.

Fig. 5. N 1s oscillator strength spectra of nitrobenzene, aniline, and methyl amine (digitized from ref. 45), derived from ISEELS. The hatched lines indicate IPs estimated from XPS (36). See Fig. 1 caption for experimental details.

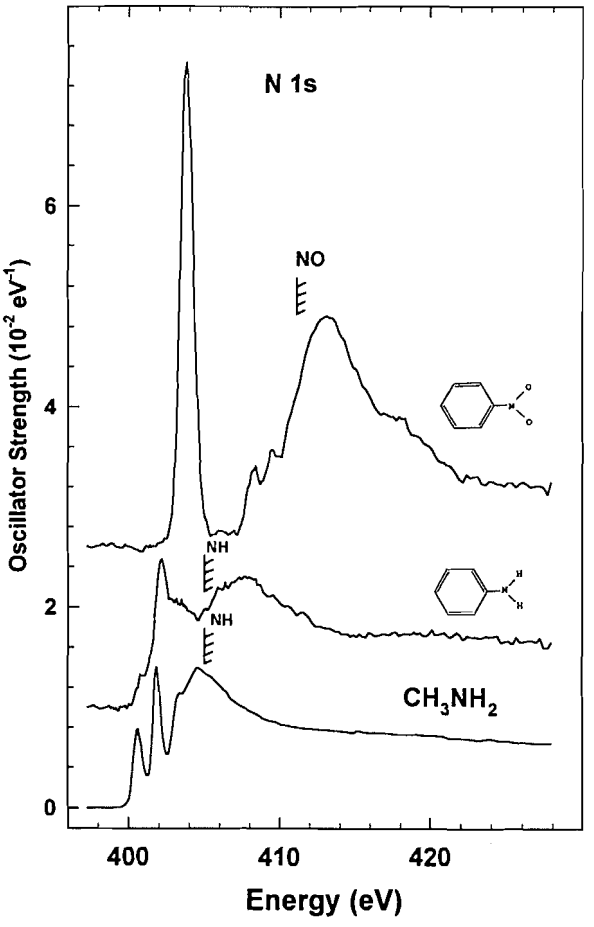

Fig. 6. N 1s oscillator strength spectra of the isomeric nitroanilines compared to a simulation that is the sum of the N 1s spectra of nitrobenzene (shifted by −0.3 eV) and aniline (shifted +0.7 eV), aligned at the estimated N 1s(NH_2) and N 1s(NO_2) IPs (2), which are indicated by the hatched lines.

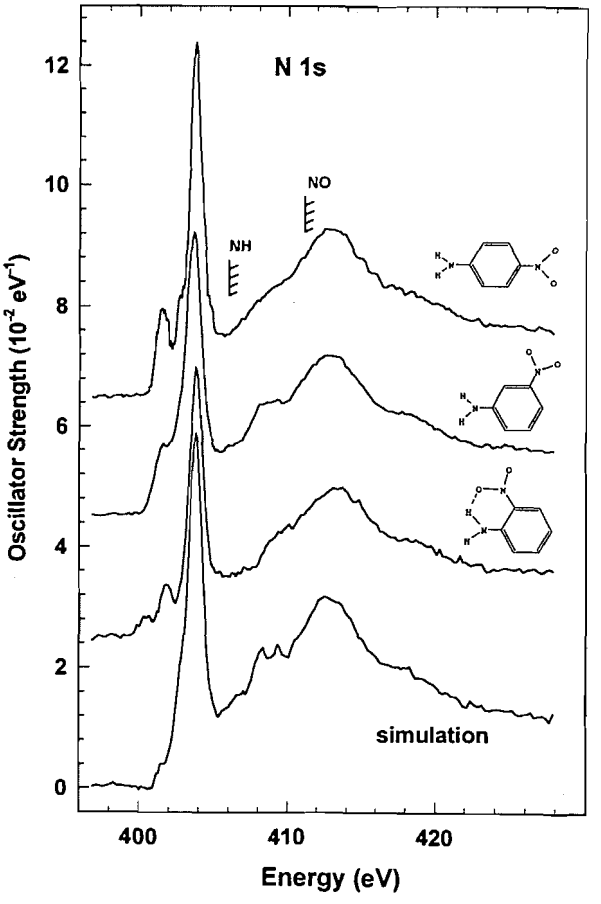

assignments of the experimental spectra, which are outlined in detail in Tables 5–7.

B. N 1*s* spectra

B.1 Aniline and nitrobenzene: monosubstituted models

Figure 5 plots the N 1s spectra of nitrobenzene and aniline. The N 1s spectrum of methyl amine (digitized from ref. 45) is also plotted in order to investigate possible effects of delocalization of the ring π^* orbitals onto the amine group. Energies, term values, and proposed assignments are given in Tables 1 and 2.

The dramatic difference between the N 1s spectra of aniline and nitrobenzene is associated with the essentially saturated character of the NH_2 group and the unsaturated character of the NO_2 group. Thus the N 1s spectrum of nitrobenzene is dominated by the strong N 1s $\rightarrow \pi^*_{NO}$ transition at 403.8 eV whereas the discrete structure in the N 1s spectrum of aniline is much weaker and can be interpreted as mainly Rydberg/σ^*_{NH} in character, as supported by the similarity of the discrete regions of the N 1s spectra of aniline and methyl amine. The N 1s continuum of aniline exhibits a broad feature centered at 407.6 eV, which is attributed to the N 1s $\rightarrow \sigma^*_{CN}$ resonance. It occurs at higher energy than the corresponding σ^*_{CN} resonance in methyl amine (404.6 eV), consistent with the shorter C—N bond length in aniline (1.431 Å) as compared to that in methyl amine (1.465 Å). Nitrobenzene has its main σ^*_{NO} resonance at 413.2 eV, with a weaker second resonance at 418.5 eV. According to the bond length correlation (43) there should only be a single N 1s $\rightarrow \sigma^*_{NO}$ resonance. However, this ignores delocalization effects, which, in molecules like CO_2 and NO_2, leads to a breakdown of the local bond picture of core excitation (46). Thus the higher energy band at ~418 eV is attributed to a second σ^*_{NO} resonance. The two σ^*_{NO} resonances are analogous to the σ_g^* and σ_u^* resonances in CO_2 (46), i.e., orbitals that can be described as positive and negative combinations of two localized σ^*_{NO} orbitals (see Sect. C for further discussion and a comparison to the corresponding O 1s $\rightarrow \sigma^*_{NO}$ features). The lower energy continuum band in nitrobenzene (413.2 eV) will also contain contributions from N 1s $\rightarrow \sigma^*_{CN}$ excitations. The positions predicted from the bond length correlation for the σ^*_{NO} and σ^*_{CN} resonances are 413 eV and 411 eV, respectively (R_{N-O} = 1.218 Å, R_{C-N} = 1.478 Å), in reasonable agreement with experiment.

B.2 N 1s spectra of nitroanilines

The N 1*s* spectra of the nitroanilines are presented in Fig. 6 while the energies, term values, and proposed assignments are summarized in Tables 5–7. Figure 6 also contains a simulated

spectrum, which is the sum of the N 1s spectra of aniline shifted up by 0.7 eV, and nitrobenzene shifted down by 0.3 eV, to account for differences in the IPs. As with the C 1s spectral simulation, if there was negligible interaction between the two substituents one would expect the measured N 1s spectra of the nitroanilines to be similar to this simulated spectrum. The poor agreement, particularly in the region below 403 eV, indicates there is significant electronic interaction between the NH_2 and NO_2 groups. The deviations from the simulated spectrum are thus a manifestation of the donor–acceptor character of nitroanilines.

While the main features of the N 1s spectra of the three isomeric nitroanilines are similar (because of the dominance of the strong N 1s(NO_2) components) there are significant differences in the weak features between 400 and 403 eV that are associated with N 1s(NH_2) excitations. The main spectral feature around 404 eV is clearly the π^*_{NO} resonance. The N 1s continuum contains three broad resonances. The broad, lower energy feature, which is considered to extend from 406 to 410 eV, corresponds to the N 1s $\rightarrow \sigma^*_{CNH}$ transition in aniline and the σ^*_{CNO} resonance in nitrobenzene. The two higher energy features (~413, ~418 eV) correspond to the two continuum resonances in nitrobenzene. With regard to our initial motivation to search for evidence for strong shake-up effects analogous to those seen in XPS, if there was an abrupt threshold onset to the {N 1s(NH_2)$^{-1}$, (π^{-1}, π^*)} shake-up process this would appear as a continuum rise around 414 eV. While there are indications of a weak shoulder at this energy, particularly in the *ortho* and *para* species, these signals are quite weak. Clearly multi-electron excitations are much weaker than the corresponding $\pi \rightarrow \pi^*$ satellite signal in core ionization of nitroanilines (11, 12).

Although the main features of the N 1s spectra can be interpreted in terms of N 1s(NO_2) excitation as outlined above, there are notable differences among the N 1s(NH_2) signals in the nitroanilines. From XPS (1–11) the N 1s(NH_2) component is expected to be more sensitive than the N 1s(NO_2) component to charge transfer interactions between the amine and nitro groups. Of course, these interactions will depend on the substitution pattern. Clearly the lower energy part of the N 1s spectrum is strongly dependent on the pattern of substitution. Initially we were puzzled as to how to interpret this part of the N 1s spectra. If the peaks at 401.6–401.8 eV are correlated with the lowest energy N 1s $\rightarrow$ 3s peak in aniline (which is suggested by similarity in term value), then there is a large intensity enhancement. One then has difficulty in assigning the weak peak observed around 400 eV in *ortho*-nitroaniline. Alternatively one could correlate the 401.6 eV peak in the nitroanilines to the main discrete N 1s $\rightarrow$ 3p/π^* peak in aniline and the 400 eV peak to the lowest energy (3s) band in aniline. With this assignment the absence of the (3s) peak in the *meta* and *para* isomers is puzzling. Neither of these trial assignments are considered acceptable. A different and more satisfactory interpretation is provided by comparison with the EHMO calculations.

B.3 Comparison to N 1s EHMO predicted spectra

Figure 7 plots expanded presentations of the N 1s spectra of the five molecules, in comparison to the N 1s predictions from EHMO. As with the C 1s region, there is reasonable agreement between calculation and experiment. The N 1s spectra are

Fig. 7. (*a*) N 1s spectra of aniline, the isomeric nitroanilines, and nitrobenzene in the region below the N 1s IP, predicted from EHMO calculations. See the text and Table 8 for details of the line widths and shifts used to construct the predicted spectra. (*b*) Corresponding experimental N 1s oscillator strength spectra.

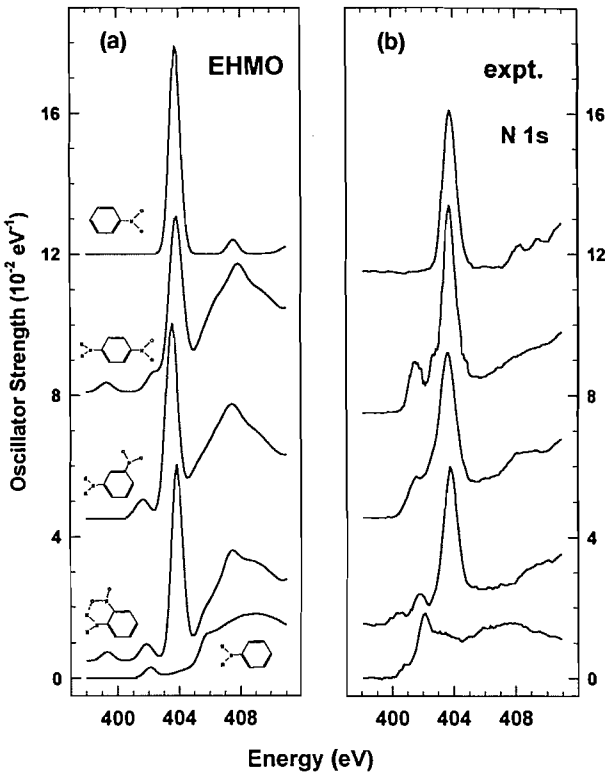

dominated by the strong π^*_{NO} and σ^*_{NO} resonances. EHMO predicts the N 1s(NO_2) component spectra contain a weak, higher energy π^* state of mixed $\pi^*_{NO}/\pi^*_{C=C}$ character that probably corresponds to the well-resolved band at 408.3 eV in nitrobenzene. The corresponding feature in the nitroanilines may exist in the 408–410 eV region but it would be masked by the N 1s(NH_2) $\rightarrow \sigma^*_{CNH}$ and N 1s(NO_2) $\rightarrow \sigma^*_{CNO}$ transitions. A similar, higher energy π^* feature is seen in the EHMO and experimental O 1s spectra (see Fig. 10 and Sect. C). While the N 1s(NO_2) $\rightarrow \pi^*_{NO}$ transition dominates the N 1s edge, there are features clearly attributable to N 1s(NH_2) excitation that EHMO reproduces quite well. In particular, the experimental pattern of the weaker features below 404 eV is also found in the calculated spectrum, with two low-lying N 1s(NH_2) peaks predicted by EHMO in *ortho*- and *para*-nitroaniline but only one in *meta*-nitroaniline. To better understand the origin of these signals it is useful to examine the MOs involved and their dependence both on substitution pattern and on the presence or absence of conjugation.

Figure 8 presents an expansion of the EHMO predictions of the N 1s(NH_2) component of the spectrum of *ortho*-, *meta*-, and *para*-nitroaniline calculated with the hydrogen atoms of the NH_2 group in the plane (the minimum energy conformation) and with the NH_2 group rotated by 90°. In addition Fig. 8 presents schematic MO diagrams of the low-energy π^* orbitals in these N 1s(NH_2) core excited species. In the planar geometry EHMO indicates there are two π^* bands with the

Fig. 8. Comparison of EHMO spectral predictions for N 1s(NH_2) → π* excitations of (*a*) *ortho*-, (*b*) *meta*-, and (*c*) *para*-nitroaniline. The upper trace in each panel is the predicted spectrum for the planar geometry while the lower trace is that calculated with the NH_2 rotated 90°, to place the H atoms out of the plane of the ring. Sketches for the lower energy π* orbitals are shown. These MO plots are projections of the 2pπ density with the diameter of the circles proportional to the 2pπ LCAO coefficient. The intensity of the peaks in the EHMO predicted spectrum is proportional to the 2pπ density on the core excited NH_2.

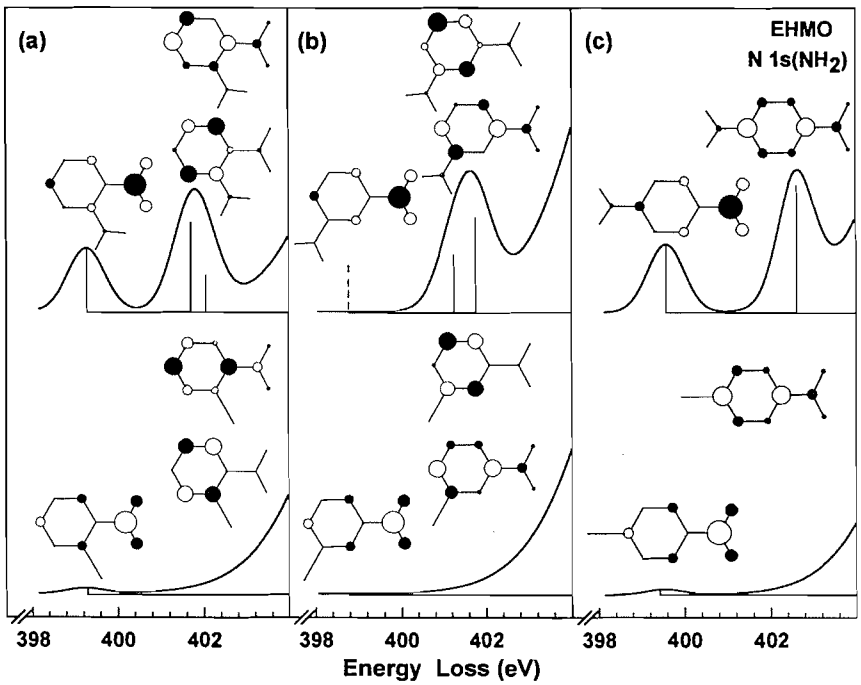

lower energy component being mainly π^*_{NO} while the higher energy component is mostly $\pi^*_{C=C}$ in character. In (planar) *meta*-nitroaniline there is only one N 1s(NH_2) → π* peak because the lower energy N 1s(NH_2) → π^*_{NO} excitation has zero intensity. When the NH_2 group is rotated by 90°, the π* delocalization is broken, the N 2p contribution to the π* orbital disappears, and the transitions are predicted to have essentially zero intensity. The EHMO results indicate that the intensity of N 1s(NH_2) → π* features in the nitroanilines and related molecules are sensitive to molecular geometry in a way that may be helpful in conformational analysis.

The agreement between EHMO and experiment for these N 1s(NH_2) excitations is surprisingly good, especially when one notes that the N 1s spectra of methylamine and aniline indicate there are significant contributions from N 1s(NH_2) → Rydberg transitions that EHMO cannot reproduce. The EHMO results for aniline (lowest curve in Fig. 7) indicate the $1\pi^*_{C=C}$ orbital has some density on the NH_2 group. This component increases considerably when the nitro group is added. The two low-lying N 1s(NH_2) excitations in *ortho*- and *para*-nitroaniline are reproduced by EHMO although the predicted separation of the two N 1s(NH_2) → π* components is larger than found experimentally. It is interesting to compare the N 1s spectra of nitroanilines with that of phenylurea (16). In both species a planar geometry leads to some $\pi^*_{C=C}$ density at the NH nitrogen atom. However the N 1s → $\pi^*_{C=C}$ transitions are much stronger in nitroaniline than in phenylurea, probably because of the strong charge-transfer coupling of the NO_2 and NH_2 groups through the ring π and π* orbitals.

It is also of interest to consider how the donor–acceptor character of these molecules is reflected in other aspects of the EHMO calculations of the core excitation spectra. Table 9 lists the total (valence electron) energy for planar and nonplanar geometries of the nitroanilines as well as a summary of the behaviour of the HOMO–LUMO gaps for different positions of the core hole in aniline, nitrobenzene and *ortho*-, *meta*-, and *para*-nitroanilines. In the neutral nitroaniline molecules the HOMO is localized on the carbons and the NH_2 (donor) substituent while the LUMO is localized on the ring and the NO_2 (acceptor) group. This expresses the donor–acceptor nature of the compound. The HOMO–LUMO gap is notably smaller in *meta*- relative to *ortho*- or *para*-nitroaniline, consistent with the less favourable situation with regard to "resonance stabilization" of the π-charge transfer (47).

The creation of a core hole changes the electron distribution in different ways. If an N 1s core hole is created on the NH_2 group, the levels with large NH_2 character are stabilized relative to those levels localized on the carbon ring or on the NO_2 group. In this situation, the charge distribution in the HOMO changes while that in the LUMO has practically the same shape as in the neutral molecules. At the same time, placing the core hole on the donor substituent increases the HOMO–LUMO gap. On the other hand, if the core hole is created on the N or O of the NO_2 group, the orbitals with NO_2 character

Table 9. Total (valence electron) energy and HOMO–LUMO gaps of neutral and core-excited aniline, nitrobenzene, and *ortho*-, *meta*- and *para*-nitroaniline from EHMO.

(*a*) Total valence electron energy, $-E$(eV).

	NH_2 in-plane			NH_2 out-of-plane		
Compound	G.S	N 1s(NH_2)	N 1s(NO_2)	G.S.	N 1s(NH_2)	N1s(NO_2)
o-Nitroaniline	981.62	998.88	996.37	981.24	998.66	995.67
m-Nitroaniline	981.82	998.86	996.34	981.32	998.66	995.73
p-Nitroaniline	981.96	998.91	996.80	981.34	998.67	995.80

(*b*) HOMO–LUMO gaps ($-\Delta E_{H\text{-}L}$ (eV)).
(*B.1*) N 1s.

	NH_2 in-plane			NH_2 out-of-plane		
Compound	G.S	N 1s(NH_2)	N 1s(NO_2)	G.S.	N 1s(NH_2)	N1s(NO_2)
Aniline	3.82	4.22	—	—	—	—
Nitrobenzene	2.24	—	0.94	—	—	—
o-Nitroaniline	1.62	1.93	0.68	1.69	2.09	0.46
m-Nitroaniline	1.37	1.82	0.23	1.73	2.03	0.50
p-Nitroaniline	1.70	2.02	0.87	1.78	2.17	0.51

(*B.2*) O 1s.

	NH_2 in-plane		NH_2 out-of-plane	
Compound	G.S	O1s	G.S.	O1s
o-Nitroaniline	1.62	1.43[a]	1.69	1.46
m-Nitroaniline	1.37	1.12	1.73	1.48
p-Nitroaniline	1.70	1.54	1.78	1.52

[a]In *ortho*-nitroaniline there is a 0.02 eV difference in $\Delta E_{H\text{-}L}$ when the O 1s hole is moved from the O atom closer to the NH_2 group to that farther from the NH_2 group. In all other cases, $\Delta E_{H\text{-}L}$ was the same for O 1s holes on each O atom.

are stabilized. In this situation the HOMO–LUMO gap decreases, facilitating the intramolecular donor → acceptor charge transfer with respect to the neutral state. In both types of core excitation the *meta* species follows a similar pattern but the HOMO–LUMO gap is smaller, reflecting less resonance stabilization. While the changing HOMO–LUMO gaps in calculations carried out on the "in-plane" geometry reflect the donor–acceptor aspect of these molecules, the situation is markedly different when the calculation is carried out with the NH_2 group rotated to remove $\pi_{C=C}/\pi_{NO}$ delocalization onto the NH_2. In the nonplanar geometry the changes with core-hole location parallel those seen in the in-plane geometry, but the HOMO–LUMO gap is similar in all three isomers. This is consistent with removing the π-delocalization component of the charge transfer.

C. O 1s spectra

Figure 9 plots the O 1s spectra of the nitroanilines and nitrobenzene, while the energies, term values, and proposed assignments of the spectral features are given in Tables 2, 5, 6 and 7. The O 1s spectra for all four species are very similar. They are dominated by the strong O 1s → π^*_{NO} transition at 531 eV. At 534 eV there is a weak feature that could be either a Rydberg state (3s, based on its term value) or a weak excitation to a higher energy π* orbital. On the basis of the EHMO results we assign the 534 eV feature to a second O 1s → π* transition. Figure 10 plots expanded regions of the O 1s spectra in comparison to the O 1s EHMO spectra. As with the C 1s and N 1s spectra, there is good agreement between the EHMO predictions and the experimental O 1s spectra. EHMO predicts a dominant O 1s → π^*_{NO} feature and a relatively strong second O 1s → π^*_{mix} transition (π^*_{mix} is an orbital of mixed π^*_{NO} and $\pi^*_{C=C}$ character). The predicted π^*_{mix} feature likely corresponds to the weak signal at 534 eV in the experimental spectrum. The O 1s EHMO spectra were also determined for the molecules with the NO_2 group rotated by 90°. In this case the π^*_{mix} feature disappears, confirming that the 534 eV feature involves π^*_{NO} delocalization onto the ring.

The O 1s continuum has two broad resonances at 538 and 541 eV, with the higher more intense than the lower energy peak. While EHMO calculations are relatively poor at predicting the *positions* of continuum features, the general shape is often reasonable and thus the calculations can provide some insight into spectral assignments. According to the EHMO calculations there are three main contributions to each of the N 1s and O 1s continua. Figure 11 plots the molecular orbitals for N 1s(NO_2) and O 1s excited *para*-nitroaniline (the EHMO results for the 1s continua are similar for the *ortho* and *meta*

Fig. 9. O 1s oscillator strength spectra of the isomeric nitroanilines and nitrobenzene derived from ISEELS. IPs from XPS (2, 36). See Fig. 1 caption for experimental details.

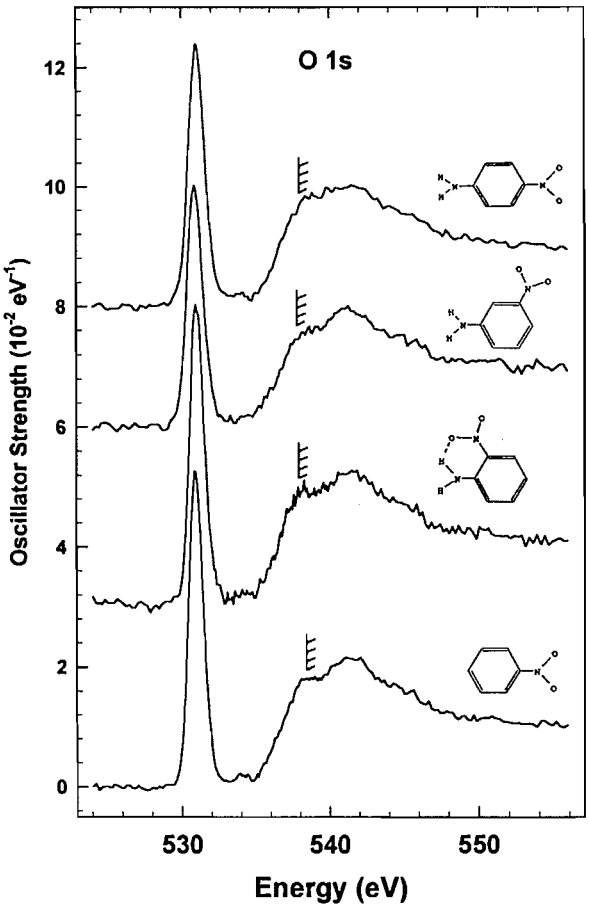

Fig. 10. (*a*) O 1s spectra of nitrobenzene and the isomeric nitroanilines in the region below the O 1s IP, predicted from EHMO calculations. See the text and Table 8 for details of the line widths and shifts used to construct the predicted spectra. (*b*) corresponding experimental O 1s oscillator strength spectra.

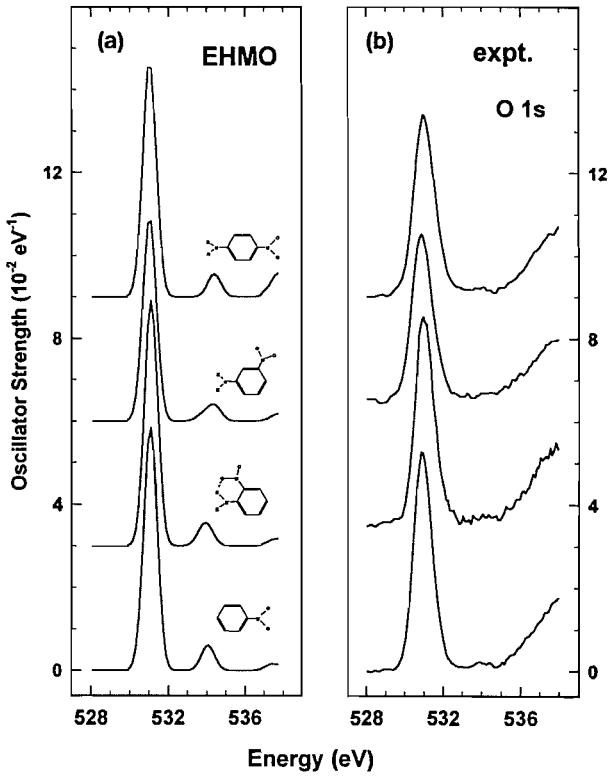

isomers). The figure shows only that portion of the MO which is critical to the core excitation under consideration. The two most intense contributions are mainly σ^*_{NO} in character, where $\sigma^*_{NO}(-)$ and $\sigma^*_{NO}(+)$ are (+/-) and (+/+) linear combinations of localized σ^*(N-O) basis functions. These are analogous to the σ_u^* and σ_g^* resonances that are observed in the O 1s spectrum of CO_2 (46). In *para*-nitroaniline these continuum orbitals have a partial π^*_{CN} and σ^*_{CN} in addition to a σ^*_{NO} character according to the EHMO calculations. In the N 1s spectrum the σ^*_{NO} features are attributed to the peaks around 413 and 418 eV. Interestingly, relative to the situation in the O 1s spectrum, $\sigma^*_{NO}(+)$ is at much lower energy than $\sigma^*_{NO}(-)$ in the N 1s spectra and thus the $\sigma^*_{NO}(-)/\sigma^*_{NO}(+)$ ordering predicted by EHMO for the O 1s spectrum is reversed to a $\sigma^*_{NO}(+)/\sigma^*_{NO}(-)$ ordering in the N 1s continuum. This is because, in the presence of a N 1s core hole, there is strong mixing with the σ^*_{CN} orbital, which leads to a much lower energy of the $\sigma^*_{NO}(+)$ orbital in N 1s core-excited than O 1s core-excited nitroanilines. The reversal of $\sigma^*_{NO}(+)/\sigma^*_{NO}(-)$ orbital ordering predicted by EHMO is a plausible explanation of the change in the relative intensities of the continuum features between the N 1s and O 1s spectra.

V. Summary

The C 1s, N 1s, and O 1s electron energy loss spectra of aniline, nitrobenzene, and *ortho*-, *meta*-, and *para*-nitroaniline have been recorded under dipole conditions and converted to oscillator strengths. The spectra do not exhibit any unusual features attributable to exceptionally strong shake-down or shake-up processes, associated either with multi-electron excitations or with the threshold of the shake-up process observed in XPS. This is consistent with electronic shielding from the core-excited electron providing strong damping of the charge-transfer relaxation process believed to give rise to signal from shake-up ion states in the XPS (1–11). Assignments for all spectral features have been proposed through a combination of analysis of systematic trends and comparison to EHMO results. The EHMO results do not reproduce completely all characteristics of the experimental spectra, but they are very useful for providing a good understanding of the effect of the core hole and for giving important insight into the interpretation of the core excitation spectra. A minor revision has been suggested to a previous assignment of the C 1s NEXAFS spectrum of solid aniline (19). The low-energy N 1s(NH_2)$\rightarrow \pi^*$ features in the N 1s spectra of the nitroanilines were found to be remarkably sensitive to the substitution pattern and the extent of π-delocalization. While some aspects of the π^* signals in the C 1s and N 1s spectra may be characteristic of ring substitution patterns it is difficult to generalize from this example because of effects specific to the nitro-

Fig. 11. Sketches of selected high-energy molecular orbitals of σ^*_{NO} character in the region of the C-NO_2 group derived from extended Hückel calculations of N 1s(NO_2) and O 1s excited *para*-nitroaniline. In each case these three orbitals are the only significant contributions to continuum resonance intensity. The vertical lines indicate the relative spacing of the orbital eigenvalues for each core excited species. A shift of 10 eV was applied between the N 1s(NO_2) and O 1s energy scales. Each orbital has large $\sigma^*_{C=C}$ components in addition to those plotted.

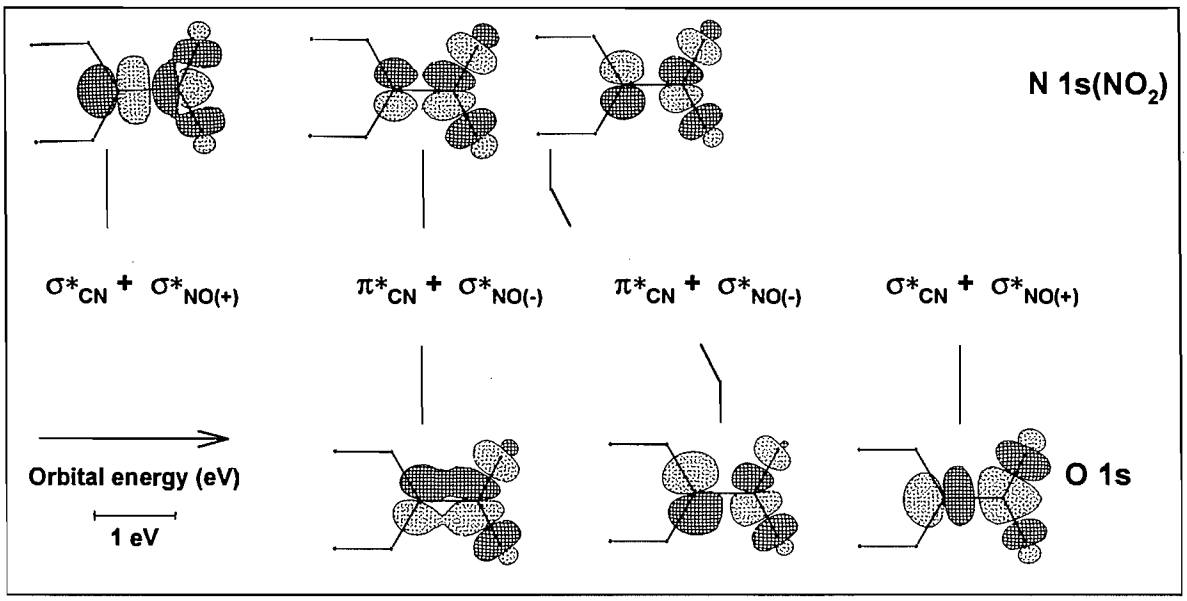

anilines, namely strong $\pi^*_{C=C}/\pi^*_{NO}$ mixing and electronic interaction through the ring π/π^* system between the donor and acceptor groups of the nitroanilines.

Acknowledgements

This work has been supported financially by the Natural Sciences and Engineering Research Council (NSERC) (Canada). C.C.T. thanks CNPq (Brazil) for support of a fellowship and S.G.U. acknowledges support of an Ontario Graduate Scholarship. We thank Dr. Meali for providing the EHMO program.

References

1. W. Domcke, L.S. Cederbaum, J. Schirmer, and W. Von Niessen. Phys. Rev. Lett. **42**, 1237 (1979).
2. M.S. Banna. Chem. Phys. **45** 383 (1980); A.R. Slaughter, M.S. Banna, and C.A. McDowell. Chem. Phys. Lett. **98**, 531 (1983).
3. M. Guerra, D. Jones, F.P. Colonna, G. Distefano, and A. Modelli. Chem. Phys. Lett. **98**, 522 (1983).
4. P.Å. Malmquist, S. Svensson, and H. Ågren. Chem. Phys. **76**, 429 (1983).
5. P.C. Ford and I.H. Hillier. Chem. Phys. Lett. **92**, 141 (1982).
6. H. Ågren, B.O. Roos, P.S. Bagus, U. Gelius, P.A. Malmquist, S. Svensson, R. Maripuu, and K. Siegbahn. J. Chem. Phys. **77**, 3893 (1982).
7. R. Nakagaki, D.C. Frost, and C.A. McDowell. J. Electron Spectrosc. Relat. Phenom. **22**, 289 (1981).
8. G. Distefano, M. Guerra, D. Jones, A. Modelli, and F.P. Colonna. Chem. Phys. **52**, 389 (1980).
9. R.W. Bigelow, R.J. Weagley, and H.-J. Freund. Chem. Phys. Lett. **82**, 305 (1981).
10. G. Distefano, M. Guerra, F.P. Colonna, D. Jones, G. Consiglio, and D. Spinelli. Chem. Phys. **72**, 267 (1982).
11. H.-J. Freund, A.R. Slaughter, S.M. Ballina, M.S. Banna, R.W. Bigelow, B. Dick, J. Lex, and H.M. Deger. J. Chem. Phys. **81**, 2535 (1984).
12. R.W. Bigelow and H-J. Freund. Chem. Phys. Lett. **77**, 261 (1981).
13. H.-J. Freund and R.W. Bigelow. Chem. Phys. **55**, 407 (1981); Phys. Scr. **T17**, 50 (1987).
14. G.R. Wight, C.E. Brion, and M.J. Van der Wiel. J. Electron Spectrosc. Relat. Phenom. **1**, 457 (1972, 1973).
15. A.P. Hitchcock, S.G. Urquhart, and E.G. Rightor. J. Phys. Chem. **96**, 8736 (1992).
16. S.G. Urquhart, A.P. Hitchcock, R.D. Leapman, R.D. Priester, and E.G. Rightor. J. Polym. Sci. Part B: Polym. Phys. **33**, 1593 (1995); S.G. Urquhart, A.P. Hitchcock, R.D. Priester, and E.G. Rightor. J. Polym. Sci. Part B: Polym. Phys. **33**, 1603 (1995).
17. H. Ade and B. Hsiao. Science, **262**, 1427 (1993); H. Ade, X. Zhang, S. Cameron, C. Costello, J. Kirz, and S. Williams. Science, **258**, 972 (1992).
18. J. Stöhr. NEXAFS spectroscopy. Springer, Berlin. 1992.
19. J.L. Solomon, R.J. Madix, and J. Stöhr. Surf. Sci. **255**, 12 (1991).
20. Y. Luo, H. Ågren, J. Guo, P. Skytt, N. Wassdahl, and J. Nordgren. Phys. Rev. A: At. Mol. Opt. Phys. **52**, 3730 (1995).
21. A.P. Hitchcock and D.C. Mancini. J. Electron Spectrosc. Relat. Phenom. **67**, 1 (1994).
22. R. Hoffmann. J. Chem. Phys. **39**, 1397 (1963).
23. R. Hoffmann. J. Chem. Phys. **40**, 2474 (1963).
24. I.N. Levine. Quantum chemistry. 4th ed. Prentice Hall, New York. 1991.
25. W.H.E. Schwarz. Chem. Phys. **11**, 217 (1975).
26. J.A. Tossel. Chem. Phys. **154**, 211 (1991).
27. A.P. Hitchcock. Phys. Scr. **T31**, 159 (1990).
28. R.N.S. Sodhi and C.E. Brion. J. Electron Spectrosc. Relat. Phenom. **34**, 363 (1984).

29. C.E. Brion, S. Daviel, R. Sodhi, and A.P. Hitchcock. AIP Conf. Proc. **94**, 429 (1982).
30. A.P. Hitchcock and I. Ishii. J. Electron Spectrosc. Relat. Phenom. **42**, 11 (1987).
31. E. Rühl, A.T. Wen, and A.P. Hitchcock. J. Electron Spectrosc. Relat. Phenom. **57**, 137 (1991).
32. A.T. Wen, E. Rühl, and A.P. Hitchcock. Organometallics, **11**, 2559 (1992).
33. J.T. Francis and A.P. Hitchcock. J. Phys. Chem. **96**, 6598 (1992).
34. C. Meali and D. Proserpio. J. Chem. Educ. **67**, 399 (1990).
35. Structure data of free polyatomic molecules. Vol. 7. Landolt Bornstein: New Series II. Springer, Berlin. 1976.
36. T. Ohta, T. Fujikawa, and H. Kuroda. Bull. Chem. Soc. Jpn. **48**, 2017 (1975).
37. B.L. Henke, P. Lee, T.J. Tanaka, R.L. Shimabukuro, and B.K. Fujikawa. At. Data Nucl. Data Tables, **27**, 1 (1982).
38. J.A. Horsley, J. Stöhr, A.P. Hitchcock, D.C. Newbury, A.L. Johnson, and F. Sette. J. Chem. Phys. **83**, 6099 (1985).
39. W.H.E. Schwarz, T.C. Chang, U. Seeger, and K.H. Hwang. Chem. Phys. **117**, 73 (1987).
40. M. Bader, J. Haase, K.-H. Frank, C. Ocal, and A. Puschmann. J. Phys. (Paris), **47**, C8-491 (1986).
41. H. Ågren, O. Vahtras, and V. Carravetta. Chem. Phys. **196**, 47 (1995).
42. S.W. Staley and A.E. Howard. Tetrahedron, **42**, 6269 (1986).
43. F. Sette, J. Stöhr, and A.P. Hitchcock. J. Chem. Phys. **81**, 4906 (1984).
44. E. Lindholm, L. Åsbrink, and S. Ljunggren. J. Phys. Chem. **95**, 3923 (1991).
45. R.N.S. Sodhi and C.E. Brion. J. Electron Spectrosc. Relat. Phenom. **36**, 187 (1985).
46. A.P. Hitchcock and J. Stöhr. J. Chem. Phys. **87**, 3523 (1987).
47. T.W. Graham Solomons. Organic chemistry. 2nd ed. John Wiley & Sons, New York. 1980.
48. S. Pignataro and G. Distefano. J. Electron Spectrosc. Relat. Phenom. **2**, 171 (1973).